Electronic Supplementary Material (ESI) for Journal of Materials Chemistry A.

Coralloid Au enables high-performance Zn-CO_2 battery and self-driven CO production

Sanshuang Gao et al.

Materials and Methods

Synthesis of coralloid Au.

In a typical synthesis, hydrophobic carbon paper (CP, SGL29BC) with 3×3 cm^{-2} geometric areas, Ag/AgCl, and carbon rod were served as working, reference, and counter electrodes, respectively. The Electrodeposition process was conducted in 10 mM $HAuCl_4$ at −0.6 V vs Ag/AgCl for 3600 s. The obtained coralloid Au was washed gently with adequate DI water and dried under a baking lamp. Finally, the as-obtained coralloid Au was tailored to 1×1 cm^{-2} for Zn-CO_2 battery/self-driven CO production and 2×2 cm^{-2} for membrane electrode assembly (MEA).

Characterizations

TEM, HAADF-STEM images, and EDX mappings of the samples were characterized by using an FEI Talos F200X S with a field-emission gun at 200 kV. XRD patterns were obtained by an X-ray diffractometer (Rigaku SmartLab) from 3 to 90 degrees at a scan rate of 20 min^{-1} with Cu Kα radiation (λ = 0.154598 nm). XPS spectra were collected by a Thermo Scientific K-alpha XPS system (Thermo Fisher Scientific, UK) with the Al Kα radiation as the X-ray source. The roughness of the electrode surface was characterized by FEI Helios NanoLab and AFM (Dimension icon). Inductively coupled plasma source mass spectrometer (ICP-MS, iCAP RQ, Germany). The liquid and gas products were characterized by Avance III HD 400MHz NMR and gas chromatography (Agilent GC-7890B).

MEA measurement.

As Fig. S6b illustrated, the CP (denotes GDL, gas diffusion layer) and coralloid Au are separated by anion exchange membrane (AEM, FAA-3-PK-130, GaossUnion) and cold-pressed together by tablet press under 5 MPa to form a membrane electrode, where the coralloid Au is sandwiched between the membrane and GDL, achieving zero distance contact. Simultaneously, the anodic

nickel foam and as-obtained membrane electrode were pressed by two pieces of bipolar plates, which possess a serpentine flow field for flowing alkaline electrolyte (1 M KOH) and 30 ml min^{-1} CO_2 gas. The as-obtained membrane electrode (2×2 cm^{-2}) covers the serpentine channel, which exposes 2 cm^{-2} valid areas to the membrane electrode of MEA. As Fig. S6c shown, silicone pads are used to seal and insulate the membrane electrode and bipolar plate. During ECR of MEA, AEM hinders a lkaline electrolyte infiltrating to coralloid Au surface and inhibits hydrogen evolution. The linear sweep voltammetry (LSV) curves were performed under 30 ml min^{-1} CO_2/Ar airflow at a sweep rate of 10 mV s^{-1} and chronoamperometry curves were measured under multiple different reduction potentials for 20 min and the optimal potential for 10 h. All the tests were connected by the two electrodes system of the Autolab electrochemical workstation (PGSTAT302N, Metrohm).

Zn-CO_2 battery measurement.

The aqueous Zn-CO_2 electrochemical was performed in H-cell, which assembles with 1×1 cm^{-2} geometric area coralloid Au immersing in catholyte (CO_2-saturated 0.5 M $KHCO_3$) as the cathode and 2×5 cm^{-2} Zn plate immersing in anolyte (6 M KOH + 0.2 M $Zn(CH_3COO)_2$) as the anode. The amphoteric electrolyte was separated by a bipolar membrane, which composites negative and positive membrane and causes H_2O dissociating into H^+ and OH^- under the direct current electric field. During the discharging process, 30 mL min^{-1} CO_2 continuously aerates into the catholyte causing CO product evolution ($CO_2 + 2H^+ + 2e^- \rightarrow H_2O + CO$) and Zn plate dissolution ($Zn + 4OH^- \rightarrow Zn(OH)_4^{2-} + 2e^-$).[S1] Regarding cathodic reaction, CO_2 reduction capably occurs in near-neutral electrolytes, which prevent acidic CO_2 from reacting with an alkaline electrolyte. For anodic $Zn/Zn(OH)_4^{2-}$, the near-neutral electrolyte is insufficient to driven Zn dissolution. Therefore, alkaline KOH and near-neutral $KHCO_3$ are adopted to actuate $Zn/Zn(OH)_4^{2-}$ and ECR,

respectively. The possible charge-discharge reactions of an aqueous Zn-CO_2 battery are assumed as below:

Cathode (0.5 M $KHCO_3$ sat. CO_2)

$CO_2 + 2H^+ + 2e^- \rightarrow CO + H_2O$

Anode (6 M KOH with 0.2 M $Zn(CH_3COO)_2$)

$Zn - 2e^- \rightarrow Zn^{2+}$

$Zn^{2+} + 4OH^- \rightarrow Zn(OH)_4^{2-}$

Overall reaction: $Zn + CO_2 + 2H^+ + 4OH^- \rightarrow Zn(OH)_4^{2-} + CO + H_2O$

During the charging process, the half-reactions on the electrode can be described as:

Cathode (0.5 M $KHCO_3$ sat. CO_2)

$H_2O \rightarrow 1/2O_2 + 2H^+ + 2e^-$

Anode (6 M KOH with 0.2 M $Zn(CH_3COO)_2$)

$Zn(OH)_4^{2-} \rightarrow Zn^{2+} + 4OH^-$

$Zn^{2+} \rightarrow Zn - 2e^-$

Overall reaction: $Zn(OH)_4^{2-} + H_2O \rightarrow Zn + 1/2O_2 + 2H^+ + 4OH^-$

Self-driven CO production measurement.

The self-driven system was assembled with two units of the above-proposed Zn-CO_2 battery and a single unit H-cell in series. For Zn-CO_2 battery modules, the anodic Zn plate, connecting coralloid Au of H-cell, serves as an electron supplier for forcing ECR occurring on the surface of coralloid Au, where 0.1 M $KHCO_3$ was saturated with 30 mL min^{-1} CO_2 gas. Regarding H-cell modules, the cathode and anode compartments were separated by Nafion 115 membrane, where coralloid Au and Pt plate occurred ECR/HER and OER in CO_2-saturated 0.1 M $KHCO_3$.

Computational details.

The DMol3 code was chosen for density functional theory (DFT) computation. Simultaneously, the generalized gradient approximation (GGA) with revised Perdew-Burke-Ernzerhof (PBE) and double numerical plus polarization (DNP) were performed as exchange-correlation functional and basis set, respectively. The self-consistent field (SCF) calculation was executed within the convergence criterion of 2.0×10^{-5}. 4.5 Å and A 15 Å were selected as the cutoff radius of the real space global orbit and vacuum slab. Finally, a 3×3×1 Monkhorst-Pack grid k-point mesh was employed during the geometric optimization.

Electrochemically active surface areas (ECSA) and Electrochemical impedance spectroscopy (EIS) measurements.

The double-layer capacitance ($C_{dl,t}$) of coralloid Au and bare CP were determined using multiple CV measurements in non-Faradaic regions at scan rates of 10-100 mV s^{-1}. According to previous literature, the double-layer capacitance of Au plate ($C_{dl,p}$) can be used to define the double-layer capacitance of ($C_{dl,t}$) Au/C electrodes.[S2] The ECSA of Au/C electrodes can be quantified by comparing their double-layer capacitances with the Au plate electrode. based on the equation: ECSA= A (cm^2) × $C_{dl,t}/C_{dl,p}$, where A is the geometric area (1×1 cm^2) of the Au/C electrode, the $C_{dl,t}$ (2.46 mF cm^{-2}) was determined using multiple CV measurements in non-Faradaic regions at scan rates of 10-100 mV s^{-1} and $C_{dl,p}$ (0.47 mF cm^{-2}) was calculated from the Source Data file of ref. S2. EIS was performed at an open-circuit potential of Zn-CO_2 battery in the frequency range from 1000 kHz to 0.01 Hz with a voltage amplitude of 10 mV.

Products analysis.

Gas chromatography (GC, Agilent GC-7890B) equipped with thermal conductivity detector (TCD) and ^{1}H nuclear magnetic resonance (^{1}H NMR, AVANCE AV III 400 Bruker) were used to analyze gas and liquid products, respectively. There are no significant peak signals of the liquid

products display in the ^{1}H NMR spectrum. Before gas products feeding to GC, all the outlet CO_2 flow rate was collected by an air pocket, which avoids extra water vapour causing the chromatographic column damage. The flow rate feeding to air pocket is equal to inlet CO_2 flow rate (i.e., the total volume of outlet gas product equals to inlet CO_2 volume). Subsequently, the collected gas product was fed to GC by the air pocket for detected the average fraction of CO/H_2. The $FE_{CO/H2}$ was described as below:

$$FE_{CO/H2}\ (\%) = (2 \times m \times F)/Q = (2C_{gas} \times V_{CO2} \times 10^{-3} \times t \times F)/24.8Q$$

where m is the mol amount of CO generated; F is the Faraday constant (96485 C mol^{-1}); Q is the total quantity of electric charge during the electrolysis at a constant current density; C_{gas} is the volume concentration of the gas-phase products, calculated based on the GC results; V_{CO2} is the flow rate of CO_2 (30 ml min^{-1}); t is electrolysis time.

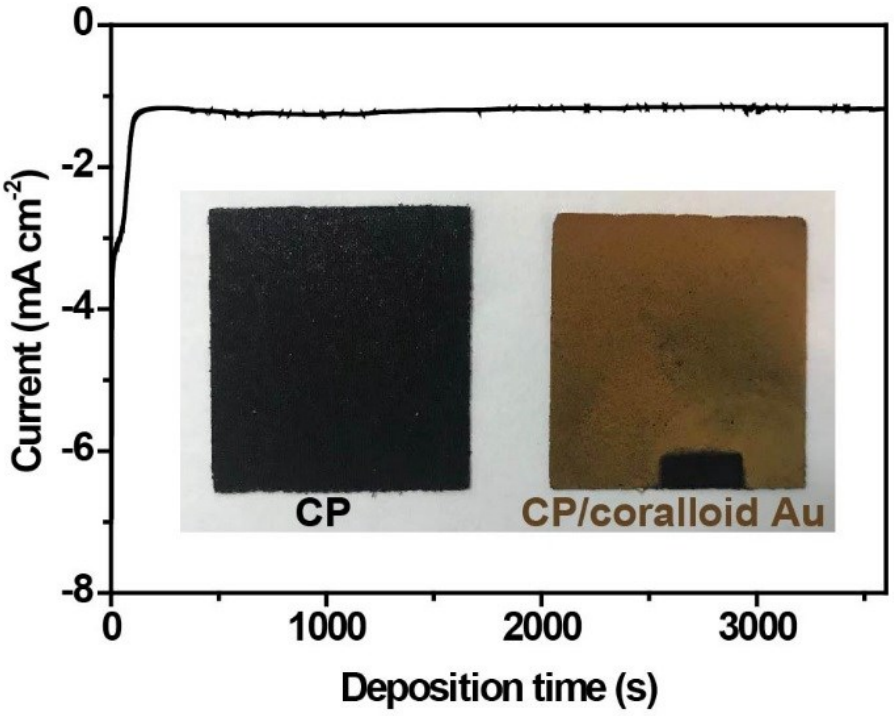

Fig. S1. The chronoamperometry curve of coralloid Au electrochemical deposition, the photograph between bare carbon paper (black, before electrodeposition) and coralloid Au (brown, after electrodeposition) is inserted in the electrochemical deposition curve for comparison.

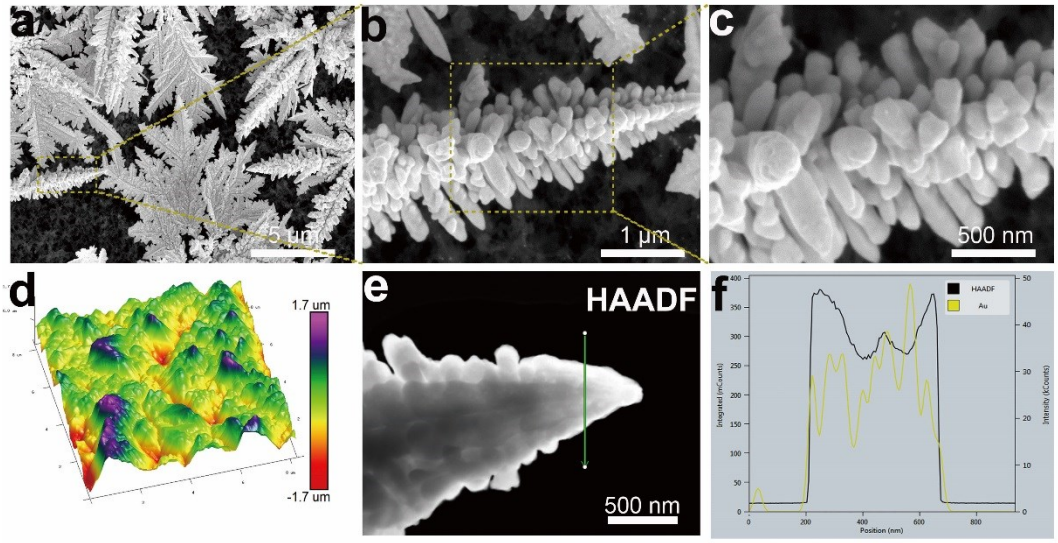

Fig. S2. The morphology characterization and element distribution analysis of coralloid Au surface, (**a-c**) SEM and (**d**) 3D AFM image characterization, (**e-f**) HAADF-STEM image corresponds with linear elemental mapping. Abundantly coralloid Au singly disperses on CP causing rough electrode surface and conforming to EDX mapping image that the thickness of Au "stem" thicker than that of Au "leaf".

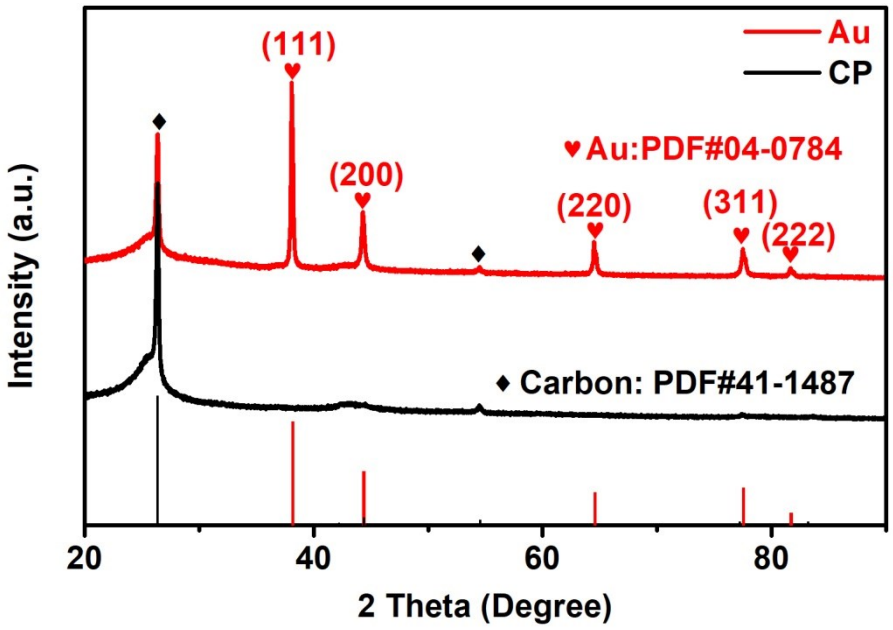

Fig. S3. The comparison of XRD patterns between bare CP and coralloid Au. Compared with bare CP, coralloid Au electrode displays additional five sharp peaks at 38.2˚, 44.4˚, 64.6˚, 77.5˚, and 81.7˚, corresponding to the (111), (200), (220), (311), and (222) planes of metallic Au.

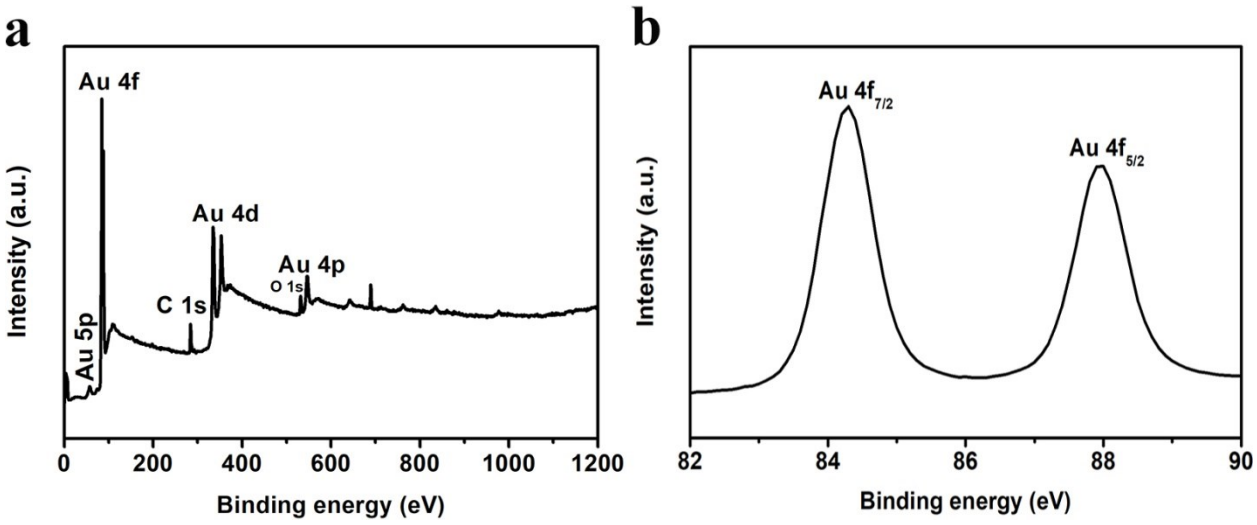

Fig. S4. (a-b) The wide and high-resolution XPS survey spectra of coralloid Au. The highest Au 4f peak can be fitted at 84.3 eV ($4f_{7/2}$) and 88 eV ($4f_{5/2}$), respectively.

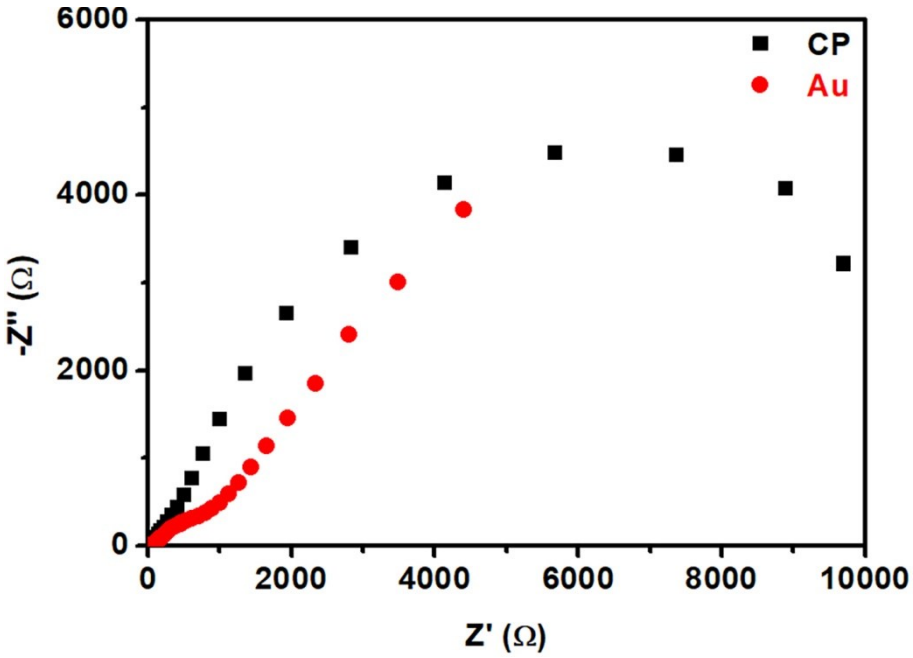

Fig. S5. The EIS measurements of bare CP and coralloid Au. Compared with bare CP, the coralloid Au exhibits a smaller semicircle in the high-frequency region, indicating coralloid Au improves the conductivity and electronic transfer kinetics of bare CP.

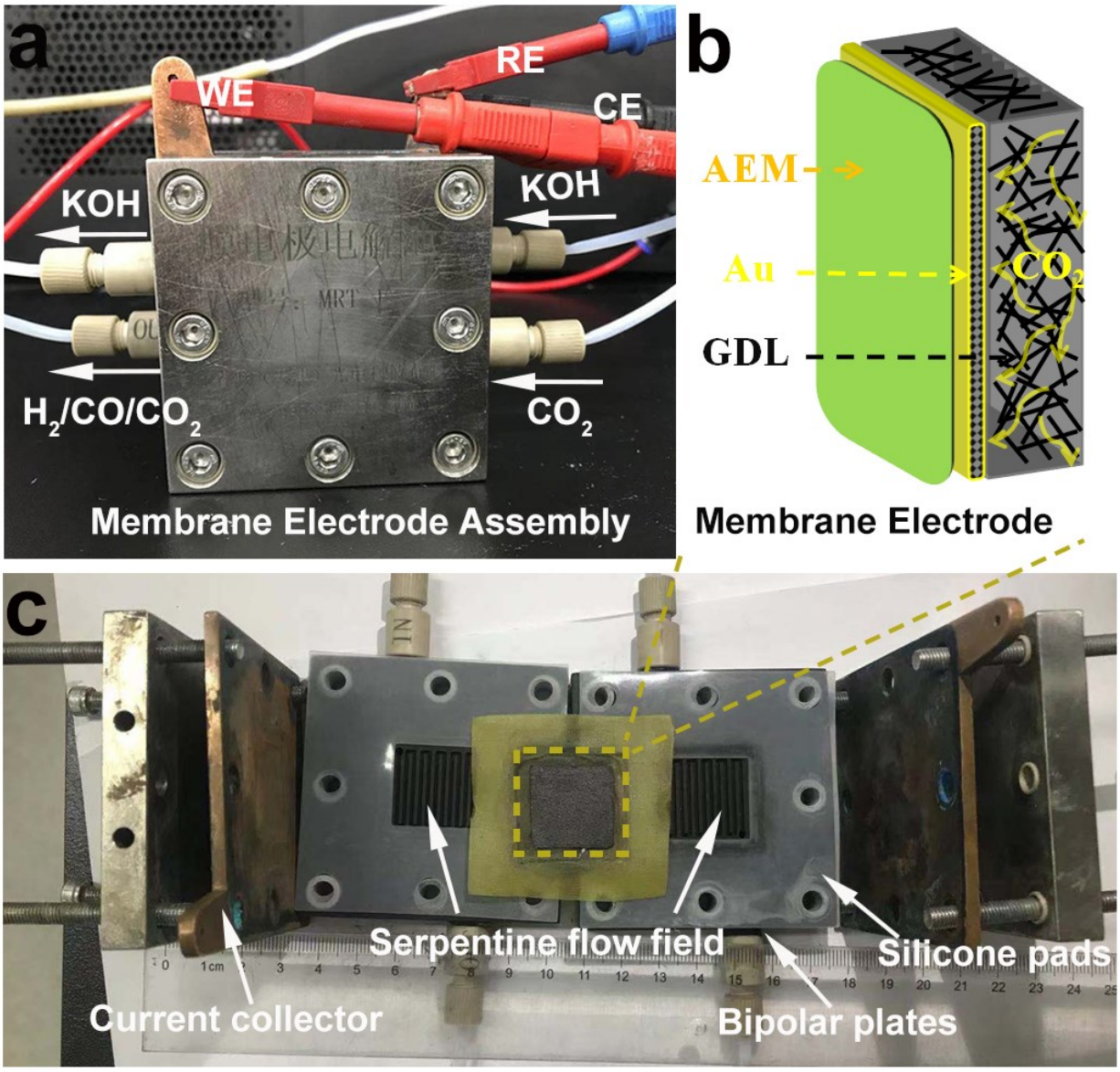

Fig. S6. (**a**) Entire and (**c**) split photograph of MEA, which is constituted of the current collector, bipolar plates and silicone pads. (**b**) the schematic membrane electrode, where CP (gas diffusion layer) and coralloid Au are separated by an AEM and cold-pressed together to form a membrane electrode (note that the coralloid Au is sandwiched between the membrane and gas diffusion layer, achieving zero distance contact). Alkaline electrolyte (1 M KOH) and CO_2 gas flow through serpentine flow fields, connecting with a two-electrode system.

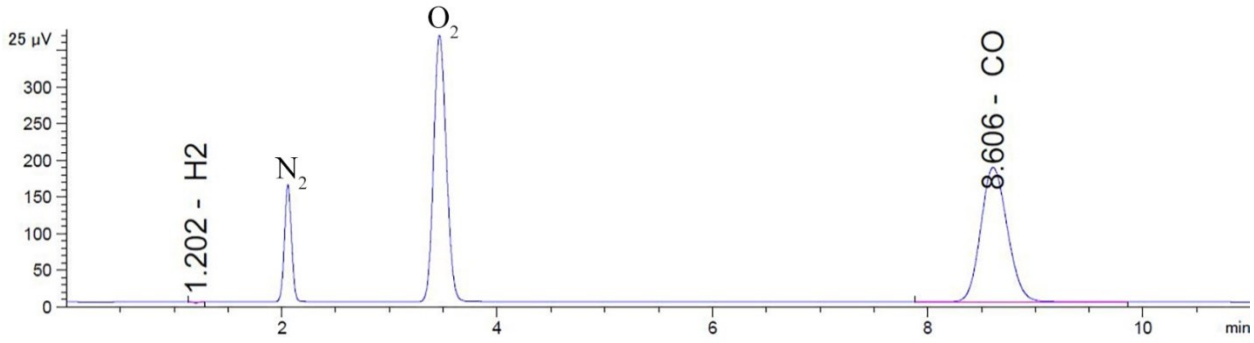

Fig. S7. Photograph of thermal conductivity detector (TCD) signal. ECR gas product, collecting from MEA at –2.4 V cell voltage, detects both H_2 and CO peaks at 1.2 and 8.6 min, respectively.

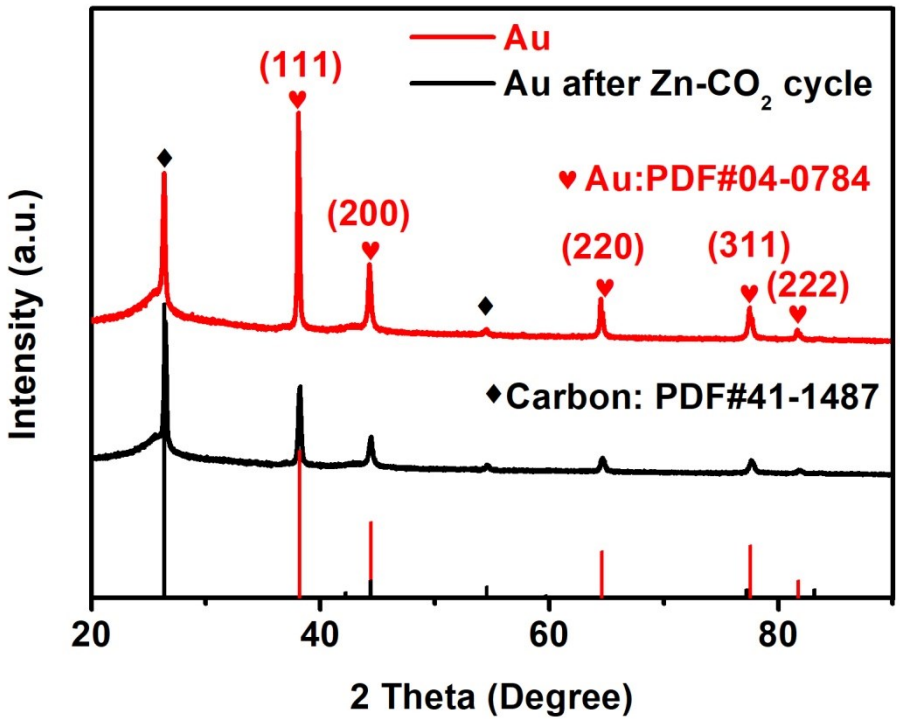

Fig. S8. The XRD patterns of coralloid Au before and after the Zn-CO_2 cycle stability test. No obvious changes can be observed.

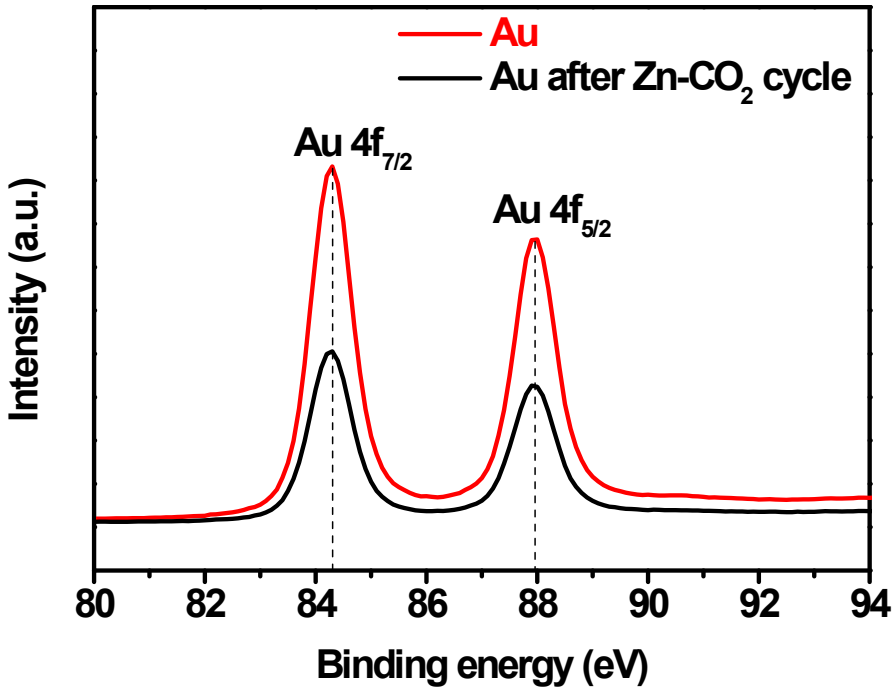

Fig. S9. The high-resolution XPS survey spectra of coralloid Au before and after the Zn-CO_2 cycle stability test. No obvious change can be observed.

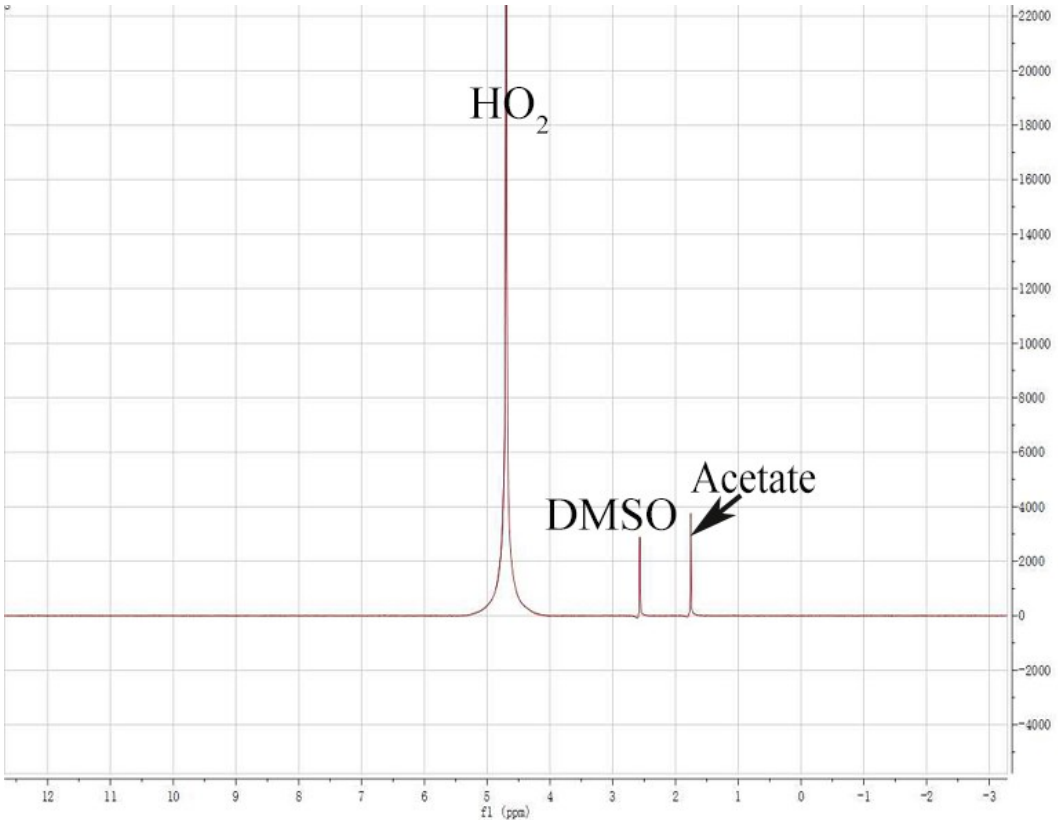

Fig. S10. ^{1}H NMR spectrum of the liquid product, collecting from the Zn-CO_2 cycle stability test, reveals that dimethyl sulfoxide (DMSO peaking at 2.6 chemical shift) and acetate (peaking at 1.87 chemical shift) were added as an internal standard, and no liquid reduction product can be detected.

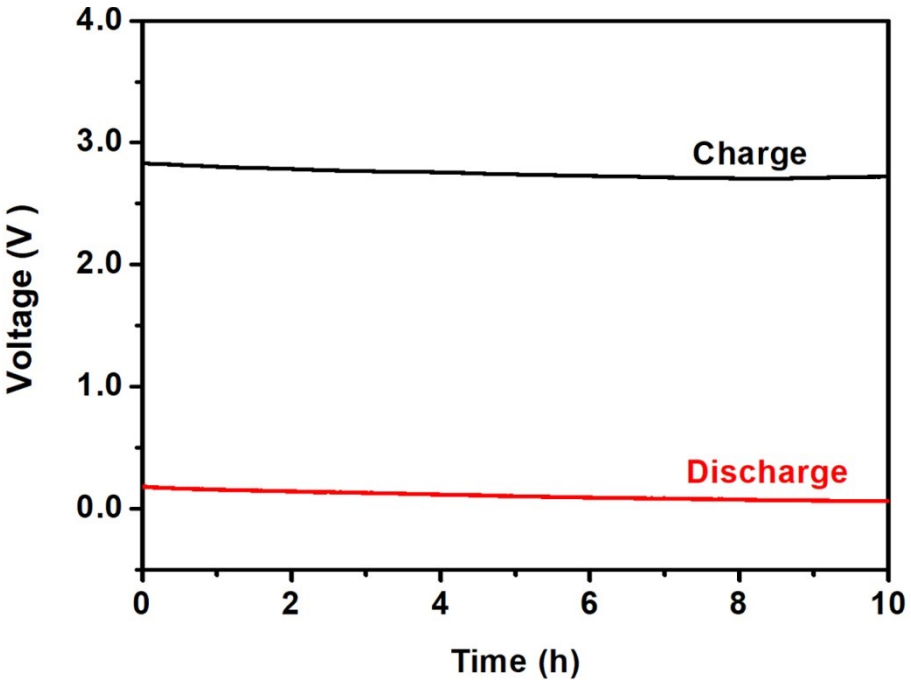

Fig. S11. The galvanostatic charge and discharge curves of the coralloid Au based Zn-CO_2 battery at 2.0 mA cm^{-2}. The battery shows good charge and discharge stability for 10 h.

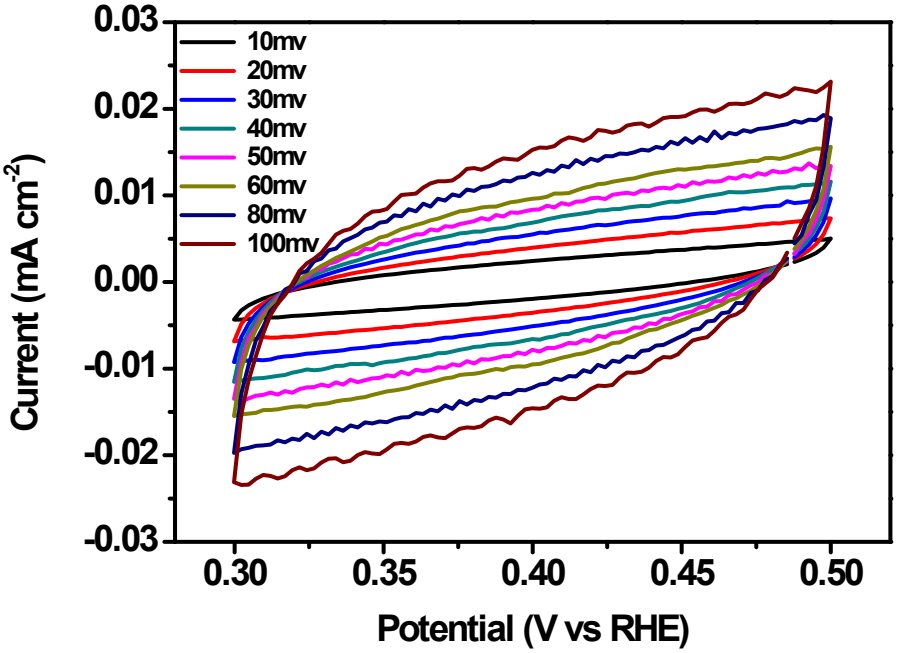

Fig. S12. The double-layer capacitance measurements of CP. Cyclic voltammetry curves were measured in non-Faradaic regions at scan rates of 10-100 mV s^{-1}.

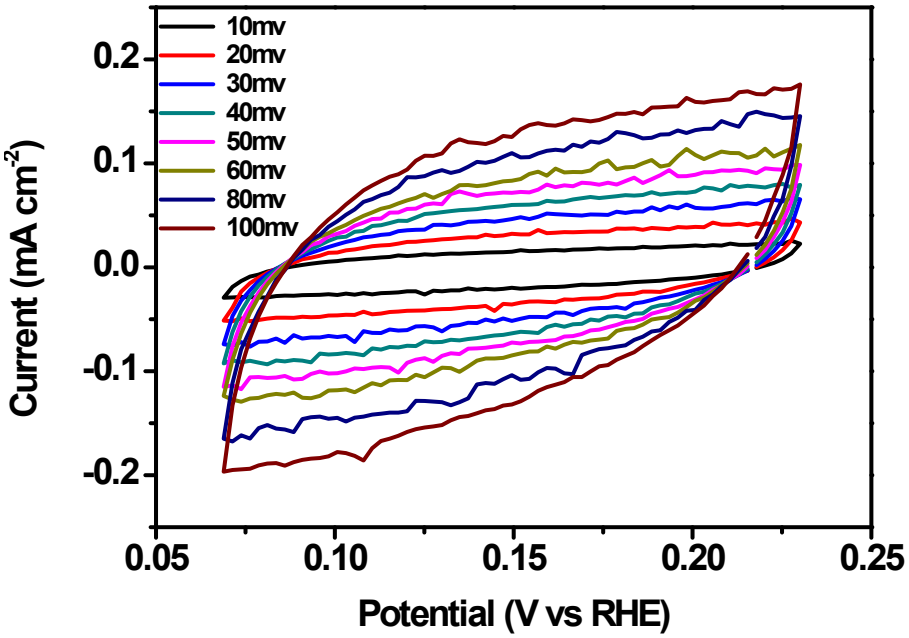

Fig. S13. The double-layer capacitance measurements of coralloid Au. Cyclic voltammetry curves were measured in non-Faradaic regions at scan rates of 10-100 mV s^{-1}.

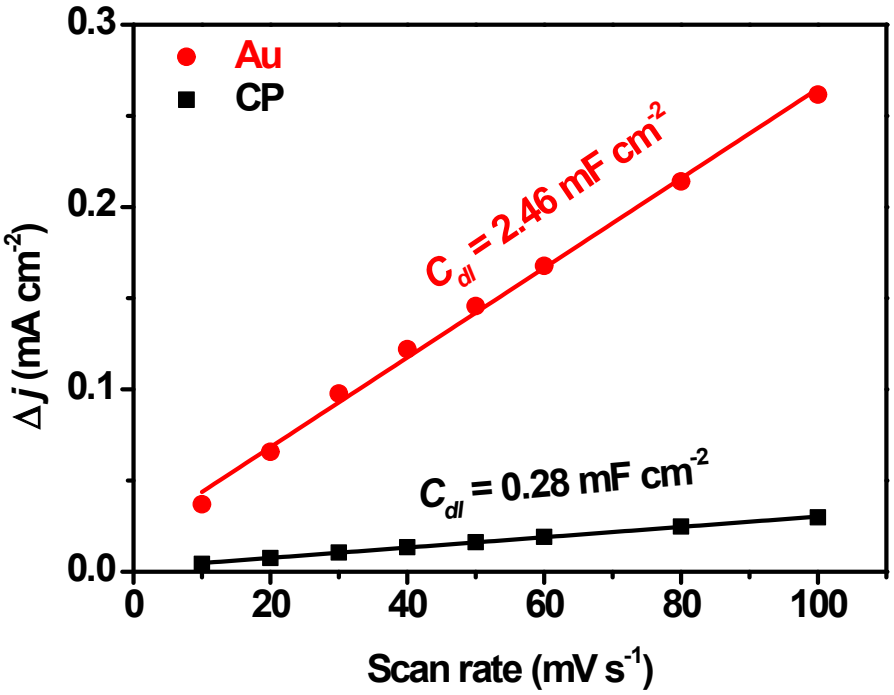

Fig. S14. The double-layer capacitance of coralloid Au and CP were plotted vs scan rate and calculated to be 2.46 and 0.28 mF cm^{-2}, respectively.

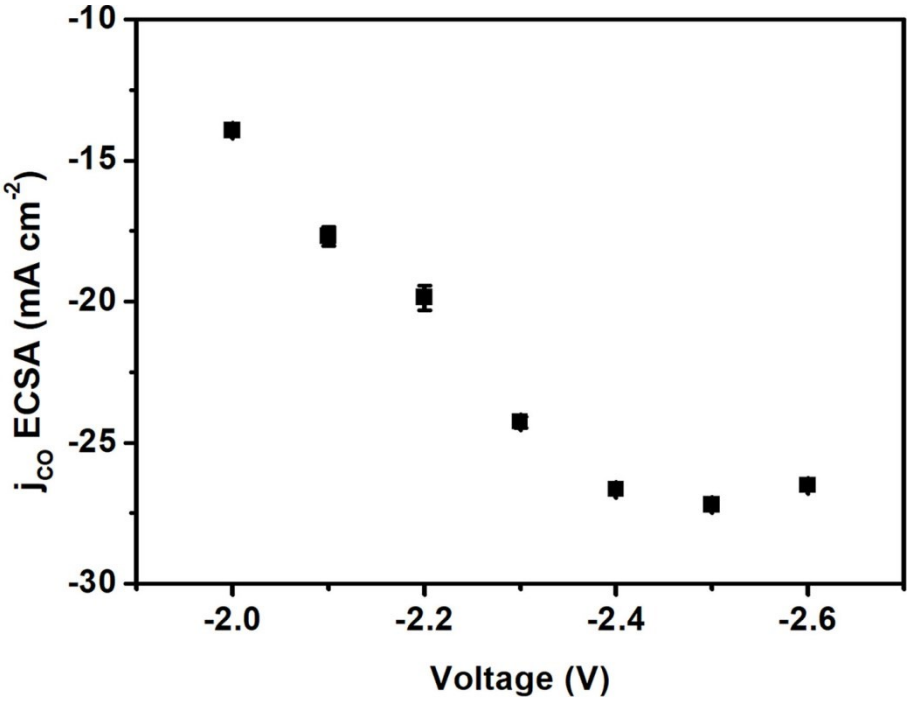

Fig. S15. ECSA-normalized j_{CO} (partial current density of CO), j_{CO} increases gradually when coralloid Au has applied a positive cell voltage before -2.4 V, conforming to the FE_{CO} growth trend.

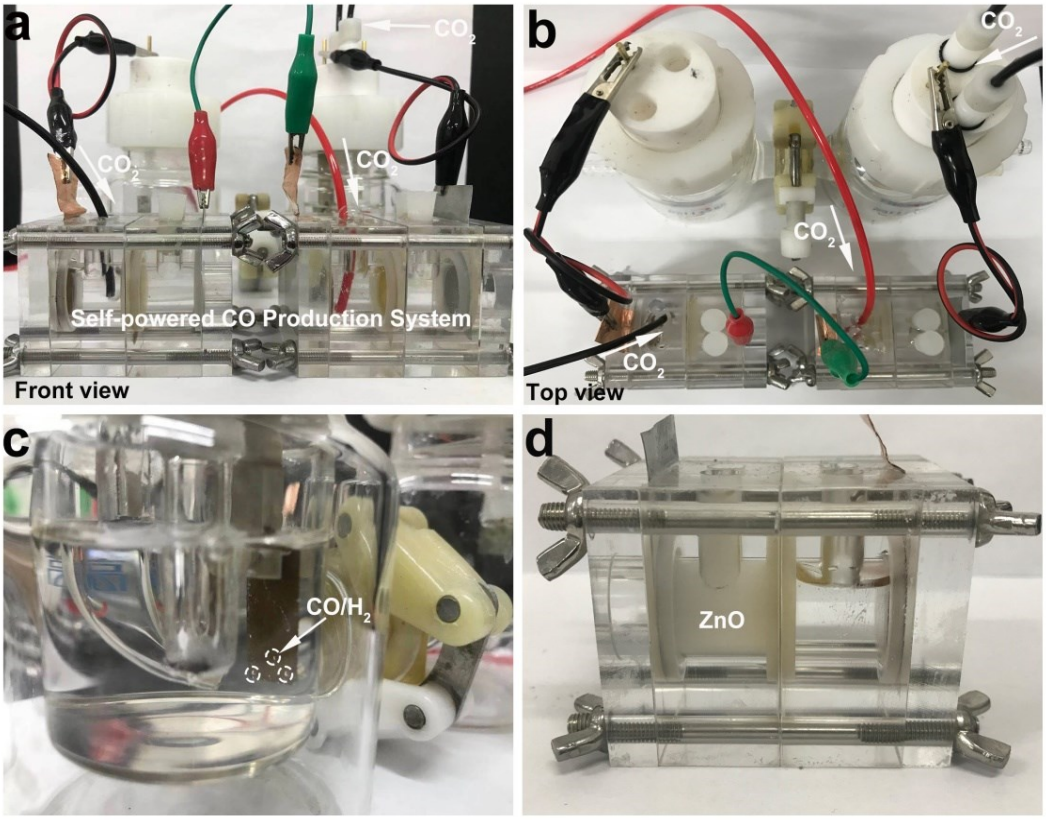

Fig. S16. Photographs of self-driven CO production system. (**a-b**) Front and top view of the self-driven CO production system couples two-unit Zn-CO_2 batteries with a single unit H-cell in series. These unit devices are saturated with CO_2. (**c**) Macro-photograph of H-cell compartment and obvious CO bubbles adhere to coralloid Au surface. (**d**) After long-term discharge, abundant zinc oxide particles uniformly suspended into the anodic compartment of a single unit Zn-CO_2 battery, indicating ECR has occurred without any external powers.

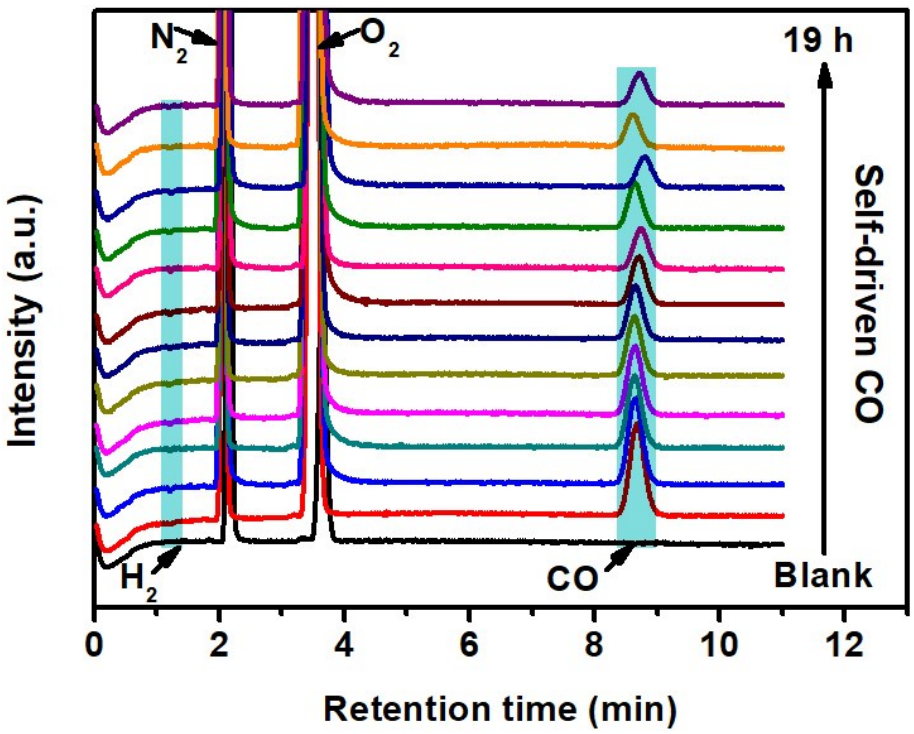

Fig. S17. Photograph of thermal conductivity detector (TCD) signal. The gas products of self-driven ECR are collected from 0.5-19 h, both H_2 and CO peaks are detected at 1.2 and 8.7 min, respectively.

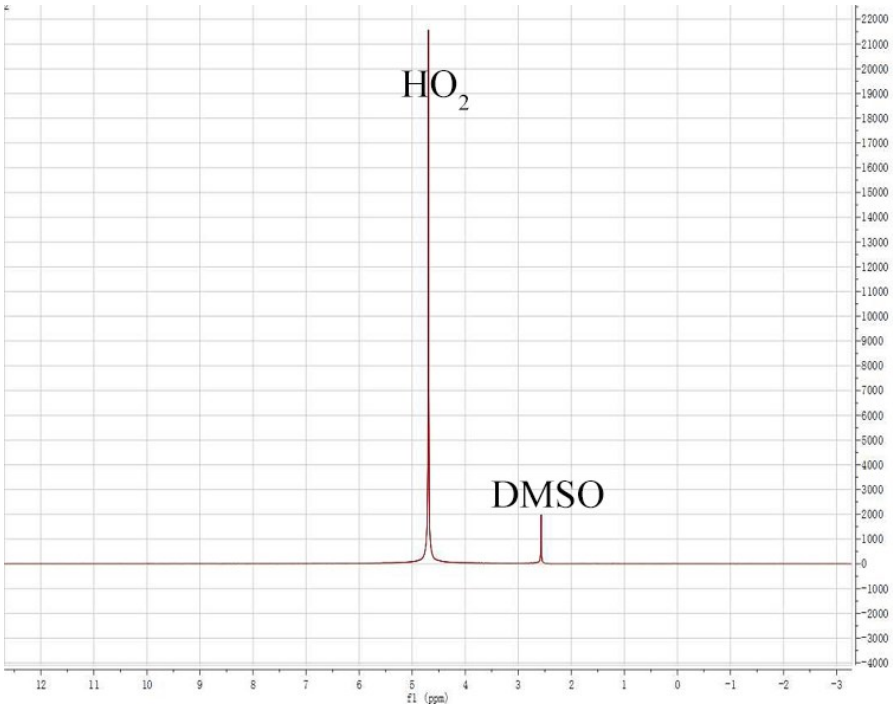

Fig. S18. ^{1}H NMR spectrum of the liquid product, collecting from the self-driven test, reveals that DMSO (peaking at 2.6 chemical shift) was added as an internal standard, and no liquid reduction products can be detected.

Table S1. Summary of reported Au catalysts for ECR performance.

Catalyst	FE_{CO} (%)	Current density (mA cm^{-2})	Reference
Coralloid Au	**96**	**-60**	***This work***
Au nanoribbons	90	-8.5	*Nano Lett.* 2020, 20, 8074
Porous Au	91	-8.3	*J. Mater. Chem. A* 2017, 5, 21955
Nanoporous Au	95	-17.5	*Appl. Catal. B-Environ.* 2018, 236, 483
Nanoporous Au	98	-12	*ACS Catal.* 2020, 10, 8860
Nano-folded Au	87	-2.4	*Nano Lett.* 2019, 19, 9154
Ultrasmall Au	83	N/A	*Nanoscale* 2018, 10, 14678

Table S2. Summary of reported aqueous rechargeable Zn–CO_2 batteries.

Cathode	[a]FE_{CO} (%)	Power density (mW cm^{-2})	Cyclability (h)	Reference
Coralloid Au	**63**	**0.7**	**86**	***This work***
NOMC	76	0.71	100	*Small Methods* 2021, 5, 2001039
Ir@Au	90	N/A	30	*Adv. Mater.* 2019, 31, 1807807
FeNC/S	N/A	0.6	25	*Adv. Mater.* 2020, 32, 2002430
Cu-N_2/GN	81	0.6	40	*Adv. Funct. Mater.* 2020, 30, 1907658
NiPG	66	~0.28	12	*J. Mater. Chem. A* 2019, 7, 2575
NiSACs	93.3	1.4	32	*Nano-Micro Lett.* 2020**,** 12, 108
Fe-N_4	87	N/A	50	*Adv. Mater.* 2020**,** 33, 2003238
Porous Pd	90(FE_{HCOOH})	N/A	33	*Angew.Chem. Int. Ed.* 2018, 5, 16996

[a]FE_{HCOOH} means the corresponding Faraday efficiency of HCOOH.

Supplementary references

[1] X. Wang, J. Xie, M.A. Ghausi, J. Lv, Y. Huang, M. Wu, Y. Wang, J. Yao, Adv. Mater. 31 (2019) 1807807.

[2] R. Shi, J. Guo, X. Zhang, G.I.N. Waterhouse, Z. Han, Y. Zhao, L. Shang, C. Zhou, L. Jiang, T. Zhang, Nat Commun, 11 (2020) 3028.